

# Internship at DTU Risø Campus: Analysis of lidar-measured wind speeds above water waves

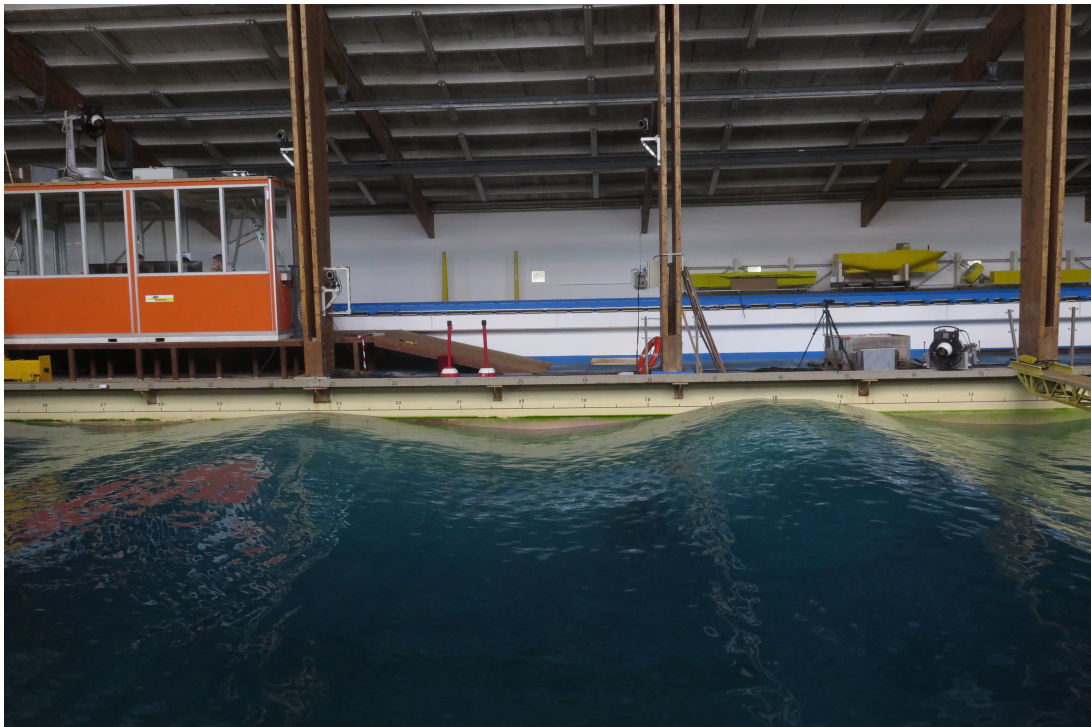
**Author:**

*Derko Budding (s1497111), University of Twente, d.j.budding@student.utwente.nl*

**Supervisors:**

*Mikael Sjöholm, DTU Wind Energy, misj@dtu.dk*

*Harry Hoeijmakers, University of Twente, h.w.m.hoeijmakers@utwente.nl*



Internship as part of Master Sustainable Energy Technology  
DTU Wind Energy Department, Roskilde, Denmark  
University of Twente, Enschede, The Netherlands

*Date: 16/12/2019*



# Nomenclature

$\lambda$	Light wave length
$c$	Speed of light in a vacuum inertial frame
$f_{S,WS}$	Sampling frequency of the WindScanner
$H_w$	Wave height in centimeters
$T_w$	Wave period in seconds
LOS	Line-of-sight speed
S(f)	Power spectrum from Fourier transformation
SA	Sonic anemometer
U	Reconstructed wind speed in x-direction
V	Reconstructed wind speed in y-direction
W	Reconstructed wind speed in z-direction
WS	WindScanner

# Contents

<b>1</b>	<b>Introduction</b>	<b>4</b>
1.1	Wind Energy . . . . .	4
1.2	Lidars . . . . .	4
1.3	WindScanner measurements . . . . .	4
1.4	Goal . . . . .	5
<b>2</b>	<b>Experiment set-up</b>	<b>6</b>
2.1	Wind-tunnel experiments in Brest, France . . . . .	6
2.2	Measurements . . . . .	7
2.3	Fourier analysis . . . . .	8
<b>3</b>	<b>Results</b>	<b>10</b>
3.1	Doppler spectra . . . . .	10
3.2	Timeseries . . . . .	11
<b>4</b>	<b>Analysis</b>	<b>14</b>
4.1	General . . . . .	14
4.2	Timeseries . . . . .	15
4.3	Periodicity of wind signal . . . . .	15
4.4	Statistical . . . . .	16
<b>5</b>	<b>Conclusion</b>	<b>18</b>
5.1	Analysis . . . . .	18
5.2	Discussion . . . . .	18
<b>A</b>	<b>Appendixes</b>	<b>20</b>
A.1	Table with variances . . . . .	20
A.2	PSD plots . . . . .	24
A.3	Matlab codes . . . . .	26
A.4	Pictures set-up . . . . .	27

# Chapter 1

## Introduction

### 1.1 Wind Energy

Wind Energy has the potential to become the largest source of renewable electrification in coming decades. Across the whole globe, nations are investing in on- and offshore wind turbines to reach certain levels of green electricity. Because of this high potential, companies and research institutes are focused on optimizing the wind energy technology in order to increase the energy output of a wind turbine. Several new projects with multiple wind turbines, also known as wind farms, are planned for the coming 20 year.

### 1.2 Lidars

The history of *light detection and ranging* (lidar) used in research goes back to the early 1960s after the invention of the laser. A globally well known *Global Positioning System* (GPS) was developed. From then on, the lidar measurement technique was developed and evolved to a renowned method in different research fields. Methods of assessing the wind resource involve the installation of tall masts equipped with cup of sonic anemometers. That is where lidars are set as a reliable alternative, reducing costs associated with masts and measuring with higher resolutions. It offers the wind industry the ability to determine the wind characteristics at substantial height using a ground-based instrument.

Lidars usually operate in the near-infra-red spectrum of light, with typical wavelengths between 750 nm and 3000 nm. It is a remote sensing technique based on the Doppler effect of a laser which gives a back-scattering while hitting particles in the air. This enables to measure wind speed in three directions, in case three lidar instruments are used. Comparing lidars with the conventional anemometers, it has to be noticed that the lidar method takes an average over a certain probe volume whereas the conventional anemometers are measuring in single point. This consequence of measuring in a larger probe volume, levels out high frequency segments in the signal.

### 1.3 WindScanner measurements

There are several commercially available WindScanners, whereas the most commonly used are the short-range (1 m - 300 m) and the long-range (5-10 km) WindScanner [6]. The short-range WindScanners are ground-based scanning lidars, whereas it measures with steerable continuous wave (CW) wind coherent lidars [2]. Compare to the long-range WindScanner, the short range wind scanners can measure on an high sampling frequency ( $>100$  Hz) and small probe volume (order of cm). The working principle of the WindScanner is simple, as it measures the Doppler shifts by comparing the frequency of the back-scattered radiation to that of the reference (outgoing) beam.

## 1.4 Goal

The main focus in this research is obtain possible improvements in wind resource measurements using the short range WindScanner. The reconstructed wind velocities are used for the main calculations. The wind data used for this analysis are reconstructed wind measurements in the wind and water tank in Brest, France [3]. The measurements were performed in November 2018. The goal for this report is to display the results in different manners, to get a better understanding of the wind behaviour above propagating water waves.

The structure of this report is first a description of the experiment set-up (Chapter 2). Furthermore a description is given how the results are established and a first quick scan is done for the data. In Chapter 4 a more elaborated analysis is performed by generating PSD plots and a comparison is made for varying input parameters. In Chapter 5 some conclusions are drawn and a discussion about the validity is displayed. This full report is a description of the work done during the internship of the author at DTU Wind Energy, Denmark from the 5th of September to 29th of November 2019.

## Chapter 2

# Experiment set-up

### 2.1 Wind-tunnel experiments in Brest, France

The main directions for this experiment can be expressed in the  $x/y/z$ -coordinates. The  $y$  coordinate represents the position in the main direction the wind. This is also the direction the water wave were propagating. Therefore this analysis will mainly focus on the velocities in  $y$ -direction. The  $x$ -coordinate is the lateral or horizontal position, whereas the  $z$ -coordinate represents the vertical position above the water level. The measurements were done in a hall which contains a water pool with a water wave generator. This generator creates water waves with a wave height up to 50 cm. A vertical moving wave measurement device was placed next to R2D2 to measure the real wave response. It is located same  $y$ -level as the WindScanner focus point,  $y = 3.0m$ . In Appendix A.4 more close-up pictures are showed.

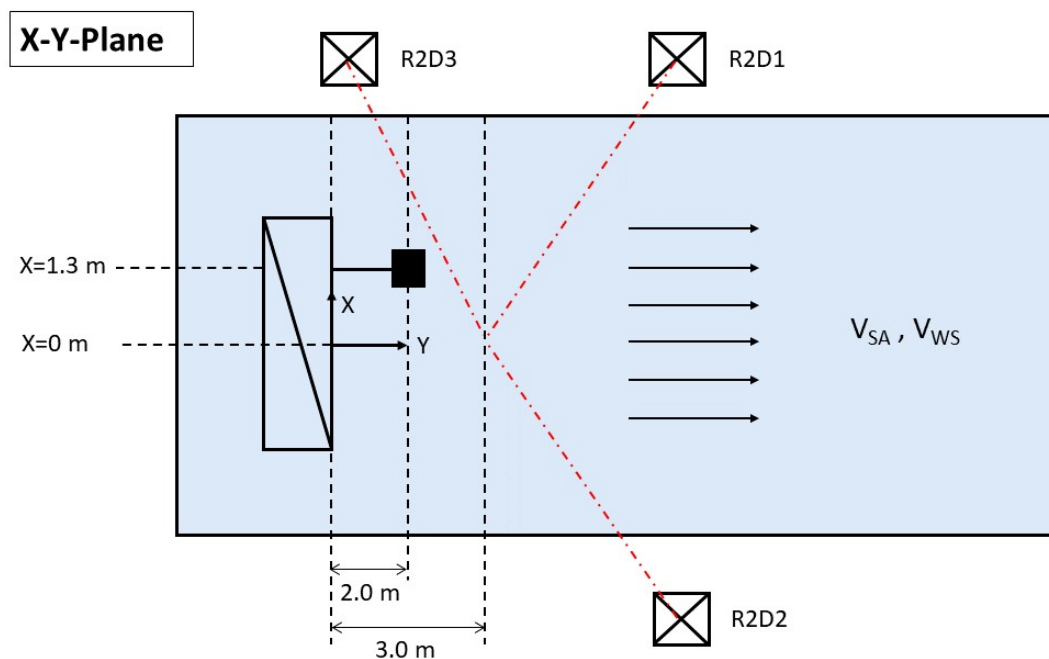


Figure 2.1: Schematic set-up for the  $xy$ -plane including the pool(blue), sonic anemometer (SA) and the three windscanners (R2D1,R2D2,R2D3).

The location of the measurements for the WS was at  $x = 0.0m$ ,  $y = 3.0m$ . Each subset of data was created by varying the wave height, wave period and mean wind speed. The height sweep was usually executed with a height resolution of either 15 or 30 cm. An overview of all datasets used for this analysis are given in Table 2.2. In addition, some plane scans were performed in all directions to determine the wind speed distributions. These results are not to be considered for this study.

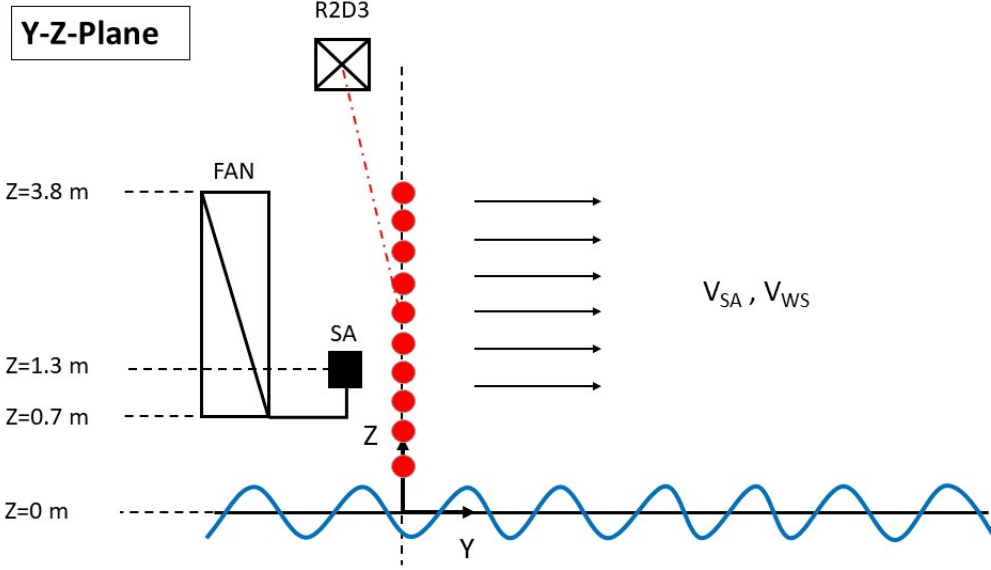


Figure 2.2: Schematic set-up for the yz-plane including the water waves(blue), sonic anemometer (SA) and the three windscanners (R2D1,R2D2,R2D3).

## 2.2 Measurements

Variable	Name	#
Dimensions test location [ $m \times m$ ]	-	25*10
Number of lidars used	$N_L$	3
Number of bins	$N_{bin}$	211
Wave length laser beam [ $m$ ]	$\lambda$	$1.565e-6$

Table 2.1: Experiment specifications

$$\Delta v = \frac{1}{2} \frac{f_{S,WS}}{512} * \lambda = \frac{1}{2} \frac{120e6}{512} * (1.565e-6) = 0.183 [m/s] \quad (2.1)$$

To account for the offset in position between the WS and SA, the delay can be calculated using the general solution of the wave propagation equation. The known values are the time period of the wave and the y-offset between SA and WS,  $\Delta y = 1.0m$ . For a water tank with infinite depth, the wave propagation speed  $V_w$  can be calculated, see Equation 2.2 . It is assumed that the fan produces an uniform flow of air and the water waves are propagating in a smooth sine wave. Therefore, the assumption is made that the time delay represents the offset in position.

$$\begin{aligned} V_w &= \frac{g}{2\pi} T_w \\ \tau &= \frac{\Delta y}{V_w} \end{aligned} \quad (2.2)$$

Using the equation for the time delay in Equation 2.2, one can calculate the values for all datasets. This is shown in the last column of Table 2.2. The Doppler spectra as an output of the WindScanner was done at a frequency of 120 MHz and a 512 point Discrete Fourier transform is performed. This leads to a velocity bin resolution of 0.183 m/s, see Equation 2.1.

Nr	$\bar{U}$ [m/s]	$T_w$ [s]	$H_w$ [cm]	res [cm]	$V_{wave}$ [m/s]	$\tau$ [s]
10	0.0	2.10	50.0	15	3.28	0.30
11	1.0	2.10	50.0	15	3.28	0.30
12	2.0	2.10	50.0	15	3.28	0.30
13	3.0	2.10	50.0	15	3.28	0.30
14	4.0	2.10	50.0	15	3.28	0.30
17	2.0	1.15	8.0	15	1.80	0.56
18	2.0	1.60	8.0	15	2.50	0.40
19	2.0	1.96	8.0	15	3.06	0.33
20	2.0	2.26	8.0	15	3.53	0.28
21	2.0	1.60	8.0	30	2.50	0.40
22	2.0	2.26	8.0	30	3.53	0.28
23	2.0	2.53	8.0	30	3.95	0.25
24	2.0	2.77	8.0	30	4.32	0.23
25	2.0	3.00	8.0	30	4.68	0.21
26	2.0	3.20	8.0	30	5.00	0.20
27	2.0	3.50	8.0	30	5.46	0.18
28	2.0	2.26	16.0	30	3.53	0.28
29	2.0	2.77	16.0	30	4.32	0.23
30	2.0	2.26	50.0	30	3.53	0.28

Table 2.2: Specifications of the timeseries performed during the experiment

## 2.3 Fourier analysis

In Lidar based experiments it is common to perform a fast Fourier transformation. This converts the timeseries from time domain into a frequency domain. To obtain the power spectra, the result of the FFT-conversion need to be scaled properly. The full working principle of this FFT is not of the interest for this research. However, before explaining the implication of FFT for this case, the general expression for the Fourier transformation  $S_X$  should be defined (see Equation 2.3). The function as defined in between the absolute brackets ( $| * |$ ), represents the FFT-function as performed in Matlab. The spectrum is analysed to the Nyquist frequency,  $N_{nyq} = f_s/2$ . Hence, the spectrum  $S_{X,k}$  for each new timeseries, K, is estimated at the frequencies as defined in Equation 2.6. The Matlab-code used to perform this Fourier transformation is given in Appendix A.3.

$$S_{X,k}(f, T) = \frac{2}{T} \left| \sum_{n=1}^N x_n \exp(-i \frac{2\pi l n}{N}) \right|^2 \text{ for } l = 1, 2, \dots, N/2 \quad (2.3)$$

$$S_X(f, T) = \langle S_{X,k}(f, T) \rangle \quad (2.4)$$

$$\sigma_X^2 = \int_{f_a}^{f_b} f \cdot S_X(f) d \log f \quad (2.5)$$

$$f_l = f_s \frac{l}{N} \quad (2.6)$$

with T the full period, i.e.  $T = f_s N$ . Where  $N$  equals the length of the input signal and  $i$  represents the imaginary part. Obviously, the output of this FFT-function returns a vector where each value is given in the form  $a+bi$  with a vector length of  $n$ . Because this conversion gives us two mirrored sets of similar data, only the left side is considered. This means only the values are used for which the frequency is below the Nyquist frequency. As can be noticed in

Equation 2.3 the squared output of the FFT is scaled by  $2/T = 2/(f_s N)$ . The factor 2 accounts for the full area under the curve, because only the left hand side of the results are used. The physical dimension of  $S_X$  after scaling is  $[m^2 s^{-1}]$ . The variance ( $[m^2 s^{-2}]$ ) of the signal can be determined by integrating over the frequency domain for  $S_X$ . Since  $S_X$  contains many orders of magnitude, the results are often displayed in semi- logarithmic scale. Since  $d \log(f) = df/f$  then  $df = f d \log(f)$ . Now pre-multiplying  $S_X$  with the frequencies and integrating over the full  $\log(f)$ -domain, the total variance can be determined, see Eqs. 2.7 and 2.8.

$$\sigma_{X,T}^2 = \int_{-\infty}^{\infty} [S_X(f)] df = \int_{-\infty}^{\infty} [f S_X(f)] d \log(f) \quad (2.7)$$

$$\sigma_{X,L}^2 = \int_{f_a}^{f_b} [S_X(f)] df = \int_{f_a}^{f_b} [f S_X(f)] d \log(f) \quad (2.8)$$

The used method with the squared values of the FFT algorithm output is commonly known as the *sampling method* [8]. The other frequently used method is the *moments method*, which is based on the mixed second order moments of the signal. For this case the sampling method has been used.

# Chapter 3

## Results

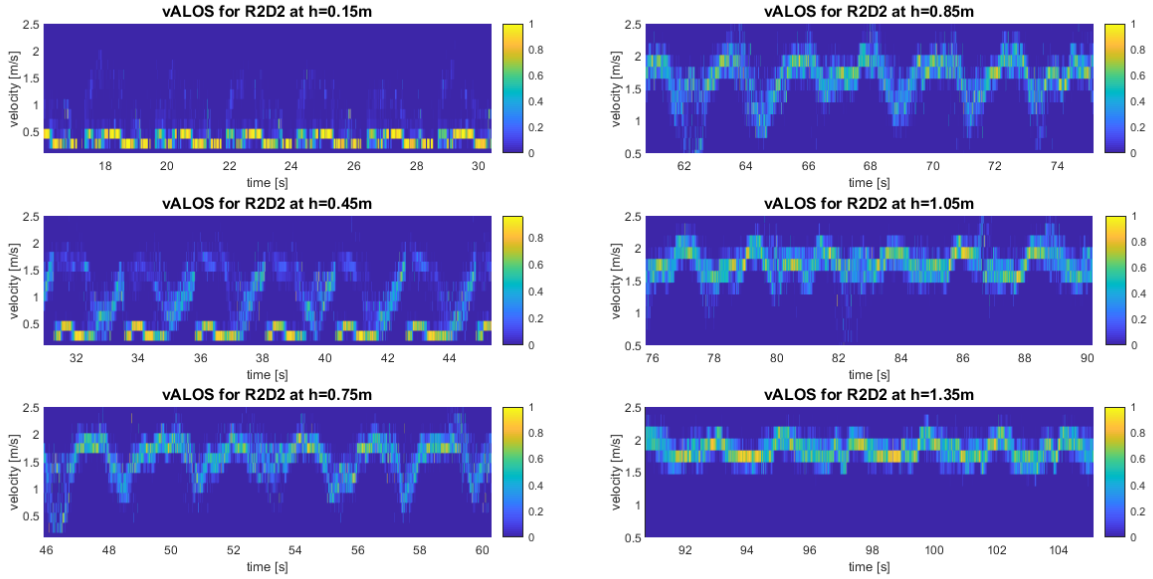
### 3.1 Doppler spectra

Post-processing of the raw data is the key in order to do a thorough analysis. Post-processing in terms of lidar based measurements using the short-range WindScanner consist of different steps. Firstly, the data acquisition unit of the WindScanner has sampling rate of 120 MHz and uses a 512 point Discrete Fourier Transform to create the laser Doppler spectrum. This output is filtered and reconstructed to obtain the reconstructed spectra. The method of average Doppler spectra is used which proved to reduce the difference in standard deviation with ordinary anemometers [1].

The most reliable frequency estimator is the median based approach to extract the line-of-sight (LOS) wind velocities of each WindScanner [7]. The LOS speeds are used to determine the radial velocities in x-, y- and z-directions. This requires some goniometric corrections using the angles between the focused laser beam and the main directions as predefined in the (Cartesian) coordinate system. This reconstruction has been done prior to the start of this analysis.

The Doppler spectra output contains 211 bins with the specific spectral resolution of 0.183 m/s as calculated in Equation 2.1. For each WindScanner (R2D1/R2D2/R2D3) at each time instant, the Doppler series is produced. The center bin with index number 106 represents the zero value. The amplitudes at these bins is the output of a Fourier transform over the Doppler shift from the back-scattered signal. The signal has been filtered which results in a set of clear signals with mainly zero values. In order to compare the spectra in a convenient way, the signal is normalized. This has been done by dividing the Doppler spectra by the sum over the full signal per time instant, as described in Equation 3.1. The R2D2 LOS speed results for dataset 30 are showed in Figure 3.1. The R2D1 LOS speed Doppler spectra show similar results, so only R2D2 is displayed. As can be seen, the water is hit at altitudes of 0.15 and 0.45 m, which indicates the clear (yellow colored) Doppler signals in the order of 0.5 m/s. It clearly diffuses the remaining wind signal. Above the mixing zone ( $h > 1m$ ), the amplitude decreases and a more harmonic signal is observed. In fact, at low altitudes there is a high probability of miscalculating the radial velocities easily. Therefore, in further analysing the data, the Doppler spectra could be separated to create two distinctive signals. For this assignment, the potential miscalculation at low heights is neglected.

$$\bar{s} = [s_1 \ s_2 \ s_3 \ \dots \ s_{211}] \cdot \left( \sum_{i=1}^{211} s_n \right)^{-1} \quad (3.1)$$



(a) LOS spectra at 0.15, 0.45 and 0.75 m

(b) LOS spectra at 0.85, 1.05 and 1.35 m

Figure 3.1: Normalized Doppler spectra for dataset 30

### 3.2 Timeseries

The first step taken in using the data, is taking the time-interval where both anemometers are running and As a result from the experiment we gained two different timeseries for both WindScanner and sonic anemometer. One can qualify this type of this data a stochastic process. The measurements are performed on time scales of 10 seconds, the variances are calculated using the Fourier transformation. Taking a first quick look at the results, one needs to be sure the sonic anemometer is synchronised with the WindScanner. In other words, one needs to be sure the measurements are performed simultaneously. Figure 3.2 shows the normalised ping response for dataset nr. 30, which will be used as a reference. In general, when the signal for the sonic anemometer is above zero and the signal for the WindScanner equals zero, both devices are running and retrieving useful data. This results in a reduced set of data containing only data within the time-series where both are switched on. Usually the water wave generator needed some time before the waves were fully developed at a constant frequency and amplitude, which differs among the different datasets.

In Figures 3.4 and 3.5 the power spectral densities are shown for dataset 30 and 22 respectively. The difference in density at the wave frequencies for the WS is factor 2 higher ( $1e - 2$  vs  $2e - 2$ ). For the other heights, the difference is even larger, see Appendix A.2. The output of the FFT-function is pre-multiplied and averaged for each height. The black line in each plot accounts for the average of the four lines plotted. This averaging is done in the log-scale frequency domain for SA and WS. The log-log scale is used to obtain the clear peak around the wave frequency ( $f_a < f < f_b$ ) and to determine the sensibility to high frequency noise in the data.

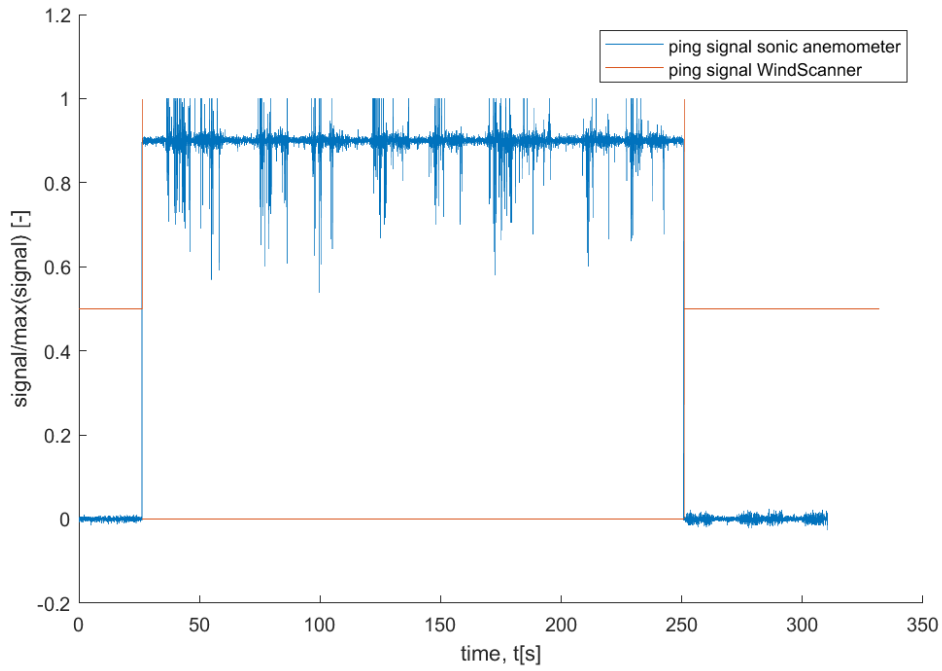
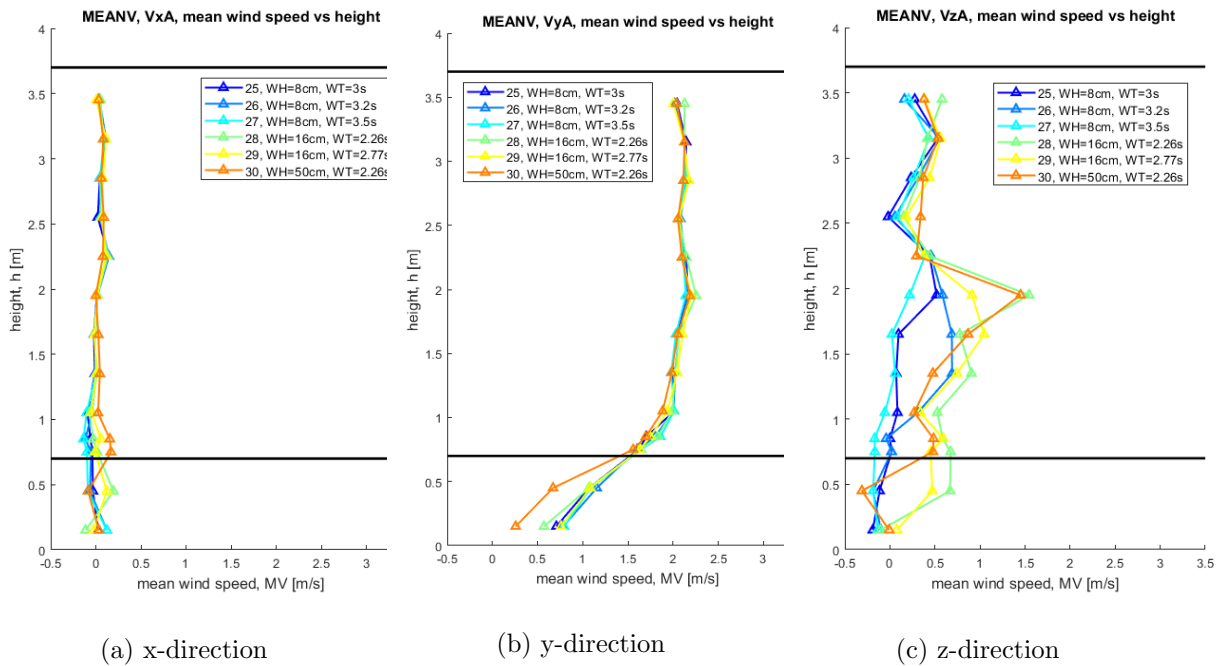


Figure 3.2: Ping signal response against time for both the sonic anemometer(blue) and the WindScanner(red) for dataset nr. 30



(a) x-direction

(b) y-direction

(c) z-direction

Figure 3.3: Shear profiles WS for dataset 25-30, height versus mean velocity

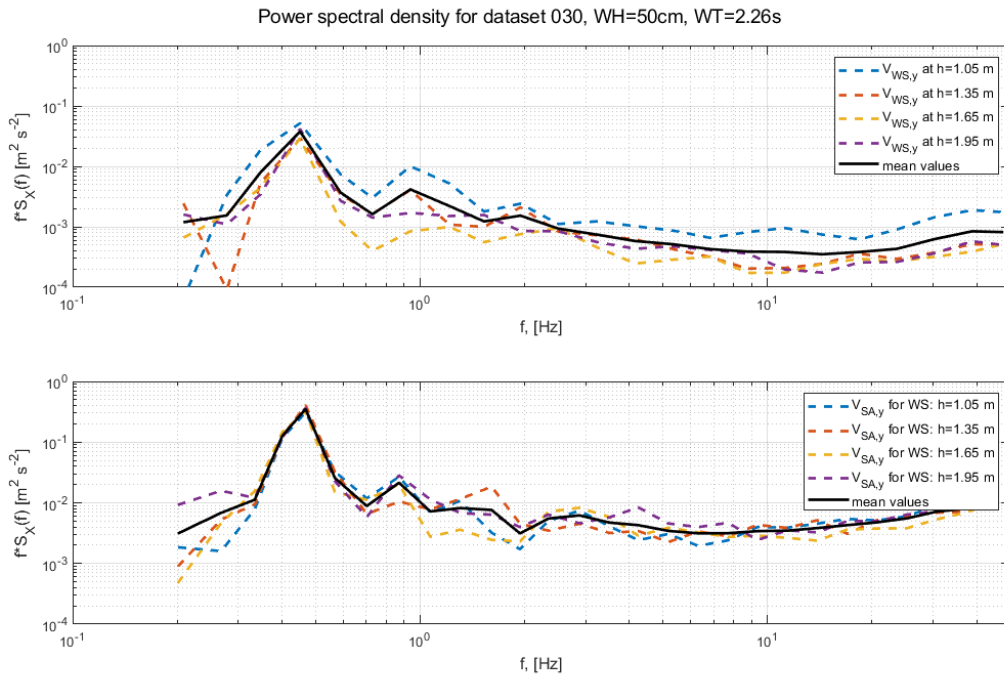


Figure 3.4: Results from WS and SA for dataset nr. 30, heights 1.05-1.95m

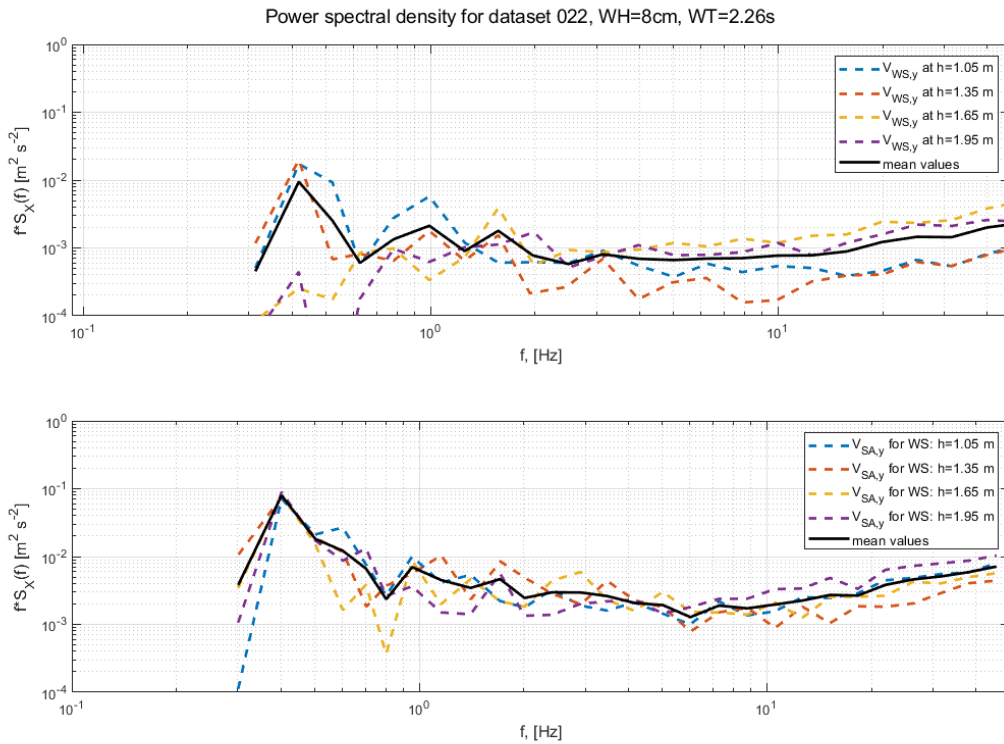


Figure 3.5: Results from WS and SA for dataset nr. 22, heights 1.05-1.95m

# Chapter 4

## Analysis

### 4.1 General

To get an in-depth insight in the data, the variance are calculated for each dataset using the pre-multiplied Fourier transforms as shown in Figure 3.4. Obviously, the measurements were performed for several heights. Using the formula for the variance as described in Chapter 3, one can create a table with the local variance, total variance and the signal-to-noise-ratio (SNR). This is shown in table 4.1. The full table for all subsets can be found in the Appendix, Table A.1.

Nr	$h[m]$	$\bar{U}[m/s]$	$T_w[s]$	$H_w[cm]$	$\sigma_X^2[m^2s^{-2}]$	$\sigma_{X,T}^2[m^2s^{-2}]$	$SNR[-]$	$V_{WS,y}[ms^{-1}]$
12	0.15	2.0	2.10	50.0	3.07	48.40	0.06	1.31
12	0.30	2.0	2.10	50.0	1.69	49.57	0.03	1.21
12	0.45	2.0	2.10	50.0	2.07	55.15	0.04	1.33
12	0.60	2.0	2.10	50.0	1.81	43.35	0.04	1.57
12	0.75	2.0	2.10	50.0	0.77	28.29	0.03	1.64
12	0.90	2.0	2.10	50.0	0.23	23.18	0.01	1.70
12	1.41	2.0	2.10	50.0	0.11	4.22	0.03	1.81
12	2.22	2.0	2.10	50.0	0.25	20.08	0.01	1.87
12	3.03	2.0	2.10	50.0	0.02	1.98	0.01	1.95
13	0.15	3.0	2.10	50.0	4.24	256.14	0.02	2.25
13	0.30	3.0	2.10	50.0	1.94	132.32	0.01	2.15
13	0.45	3.0	2.10	50.0	2.62	94.03	0.03	2.22
13	0.60	3.0	2.10	50.0	2.94	102.77	0.03	2.30
13	0.75	3.0	2.10	50.0	2.24	74.31	0.03	2.39
13	0.90	3.0	2.10	50.0	0.43	92.69	0.00	2.50
13	1.41	3.0	2.10	50.0	0.03	20.50	0.00	2.70
13	2.22	3.0	2.10	50.0	1.35	48.46	0.03	2.97
13	3.03	3.0	2.10	50.0	0.22	4.16	0.05	3.01

Table 4.1: Output for all datasets with variances for different heights

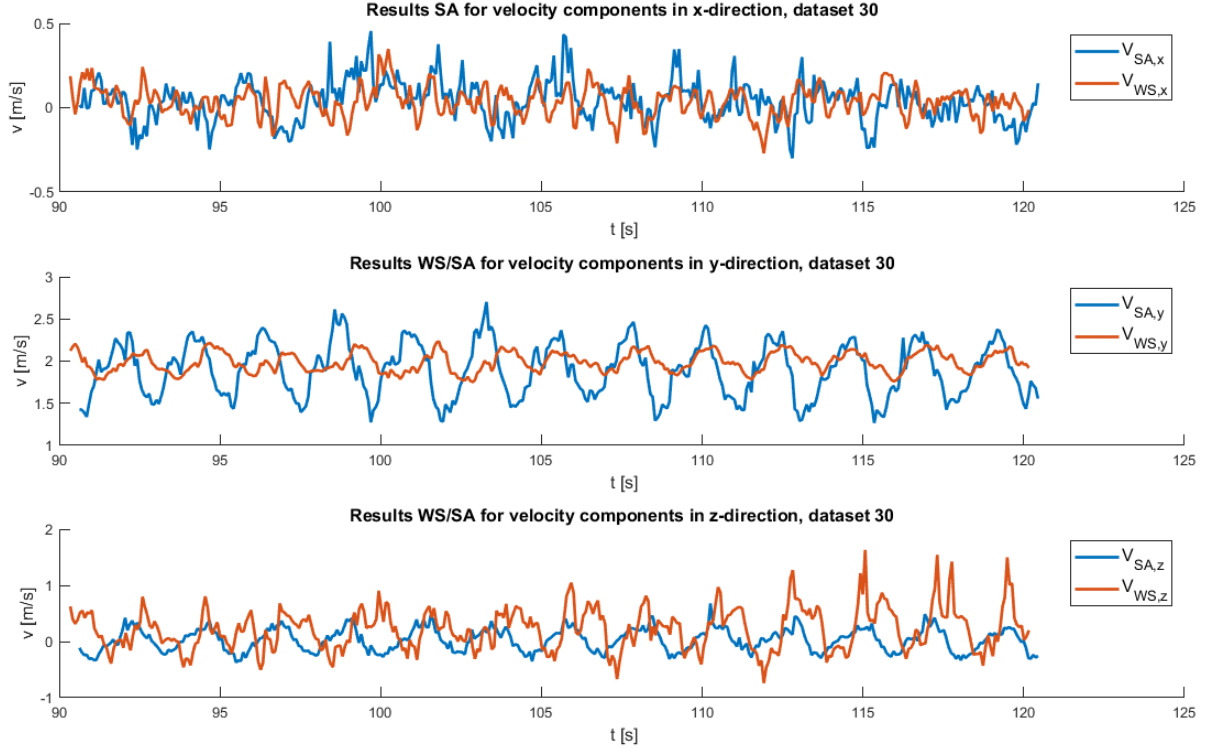


Figure 4.1: Corrected signals for dataset 30 with  $\tau = 0.283$  s, WS heights: 1.05 m and 1.35 m

## 4.2 Timeseries

In Figure 4.1 the results from both WS and SA are plotted for velocity components in all main directions. These are averaged signals, with a 0.08 s time span, containing 8 data points. The WS signal is shifted back in time with the calculated delay  $\tau = 0.183$  s. The value for  $\tau$  is calculated using Equation 2.2. Observing the second plot in Figure 4.1, the first striking difference between the two signals is the amplitude. The SA roughly has its (average) minimum and maximum at 1.5 and 2.4 m/s respectively with mean value 1.9 m/s, whereas the WS has an average minimum and maximum at 1.8 and 2.2 m/s respectively with a mean value of 2.0 m/s. In addition, after correcting the signal with the expected delay, the phase difference is still huge.

In order to explain the difference between the output of the sonic anemometer and lidar based instruments, the working principle need to be considered. Sjöholm et al. [5] showed that a spatial volume averaging effect in lidar measurements scales squared with the laser beam distance to the focus point. This could be investigated more in detail, to be sure the difference in result not solely is caused by the averaging effect in the WindScanner.

## 4.3 Periodicity of wind signal

To get a more thorough understanding of the wave propagation observed in the wind signal, the periodicity of the wave is analysed. By splitting the signal in an integer amount of periods equal to the wave period, the pattern is hopefully observed. Since the measurements were performed in 15 s intervals, the amount of periods taken into account varies from 4 ( $T_w=4.0$ s) to 13 ( $T_w=1.1$ s). The results are shown in Figure 4.3, for both WS and SA at the same time spans. In Figure 4.3a

it can be noticed that with increase in height the amplitude is changing and the boundaries of the distributions become more constant for heights above 1.35 m. At the same time instant the sonic anemometer picks up a more harmonic sinusoidal signal, despite the more extreme outliers along the period.

## 4.4 Statistical

Once the variances are calculated, the dependency on the experiment variables can be analysed. First the local variance at the water wave frequency is used. This value represents the average amplitude of the harmonic wind signal. The total variance is calculated by integrating over the full domain. This enables one to calculate the signal-to-noise-ratio (SNR) for each dataset at all heights measured. This section will present plots for the local variances, which will be plotted against the variables  $WT$  and  $h$ .

In Figure 4.2a the average mean value of the local variance is plotted against the wave height for dataset 21-30. Only the heights where the wind is assumed to be uniform is taken into account:  $1.0 < h < 3.0m$ . As the linear regression line shows, the variance is increasing for rising numbers of  $WT$ . It has to be noticed that datasets 21-27 (dark colors) with  $WH$  of 8cm show an even more linear dependency on  $WT$ . In Figure 4.2b the local variance versus height is plotted. All datasets show the same slope with the highest values at 0.5 m, which in fact is just above water level. The dark red line of dataset 30 shows the highest values at higher values for  $h$ . Due to the wave height of 50 cm, this appears to be as expected. The highest values are obtained at  $h = 0.5m$ , but it has to be noticed that at this position the mean velocity is close to zero, see Figure 3.3.

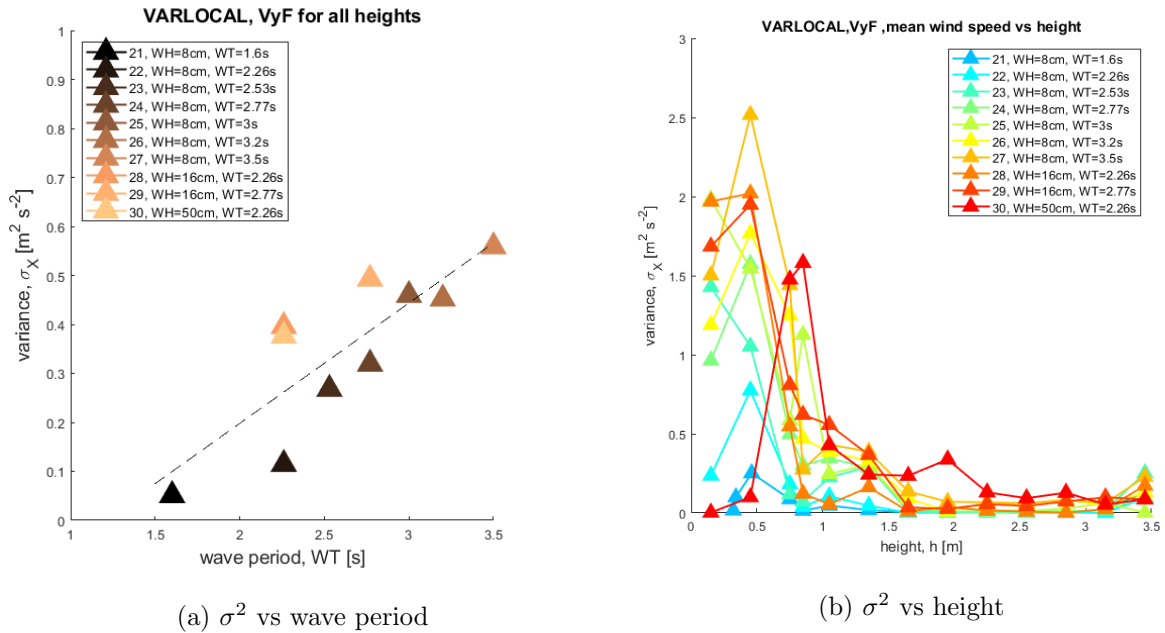
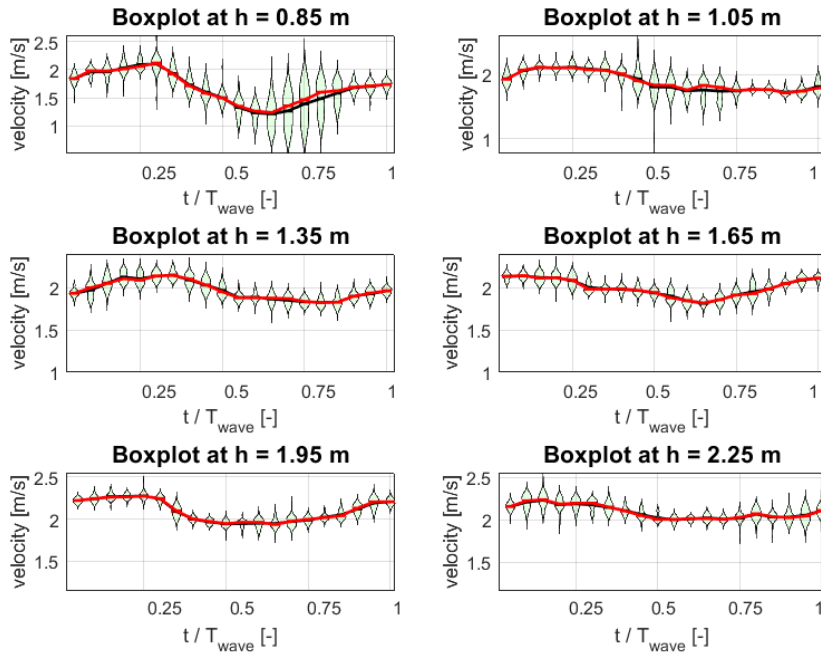
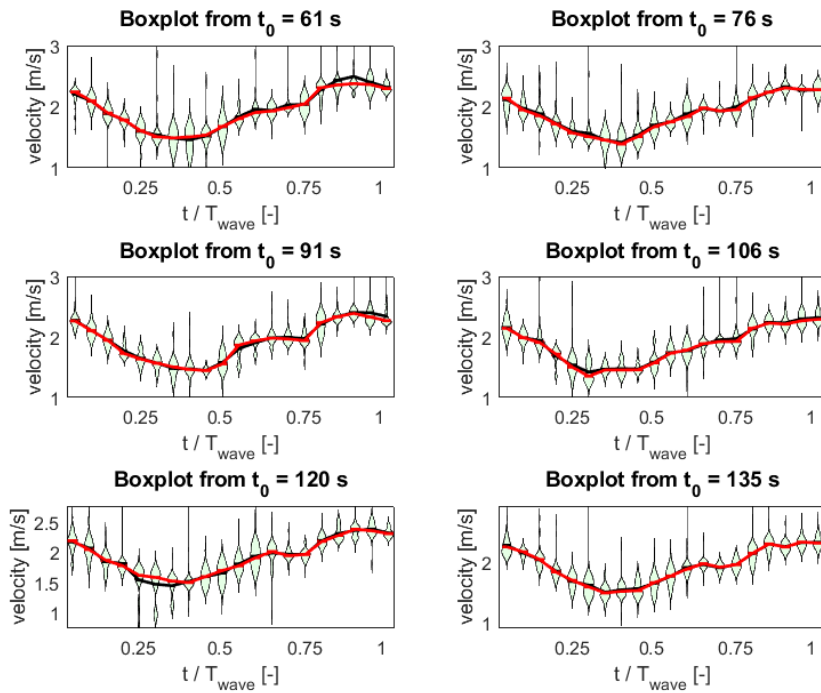


Figure 4.2: Local variances for  $V_{WS,y}$ , dataset 21-30



(a)  $V_{WS,y}$  at heights: 0.85 - 2.25 m



(b)  $V_{SA,y}$  at heights: 0.85 - 2.25 m

Figure 4.3: Distribution plots for  $V_{WS,y}$ . Distributions are 'violin'-plots to show the type of distribution, number of bins is 20

# Chapter 5

## Conclusion

### 5.1 Analysis

From the data analysis it was first presented by using the Doppler spectra. It was noticed that at z-levels just above the water level, the lidars are hitting the water and hence disturbing the wind signal. Furthermore by calculating the variances from the power spectral densities at the wave frequency, it was observed that the sonic anemometer gives higher values with respect to the WindScanner. For the WindScanner results for low wave height of 8 cm gave a clear signal which is less noisy, but the variance around this frequency was observed to be nihil. Plotting the local variances against wave period has shown an linear increase in variance for increasing numbers of wave period.

### 5.2 Discussion

The validity of the data has to be considered. First of all, the timeseries for this experiment covering 15 seconds per height. Despite the clear wave propagation observed in the wind speed signal, the time span is very small compared to a common wind resource analysis. The stochastic behaviour of a wind signal in general plays a major role, which can barely be observed in PSD plots. The 10-min averages with corresponding frequency order of magnitude of  $10^{-3}$  are usually the frequencies of interest [4]. Eventhough this experiment was done by use of a fan which could produce more or less uniform wind velocities in the main direction, the duration of the experiment should be extended draw conclusions with a high probability.

# Bibliography

- [1] Jakob Mann Nikolas Angelou Emmanuel Branlard, Anders Tegtmeier Pedersen. Retrieving wind statistics from average spectrum of continuous-wave lidar. *Atmospheric Measurement Techniques*, 2013.
- [2] Torben Mikkelsen Etienne Cheynet, Jasna Bogunovic Jakobsen. Application of short-range dual-doppler lidars to evaluate the coherence of turbulence. *Exp Fluids*, 57:184, 2016.
- [3] Ifremer. National institute for ocean science.
- [4] Mark Kelly Morten Nielsen Jacob Berg, Jakob Mann. *Micro meteorology for Wind Energy*. 2017.
- [5] Jakob Mann Karen Enevoldsen Mikael Sjöholm, Torben Mikkelsen. Spatial averaging-effects on turbulence measured by a continuous-wave coherent lidar. *Meteorologische Zeitschrift*, 18, 2009.
- [6] Torben Krogh Mikkelsen. Windscanner.
- [7] Mikael Sjöholm Michael Courtney Nikolas Angelou, Jakob Mann. Direct measurements of the spectral transfer function of a laser based anemometer. *Review of Scientific Instruments*, 2012.
- [8] Jur Vogelzang. How to calculate wind spectra. *Satellite Application Facility for Numerical Weather Prediction*, 2013.

# Appendix A

## Appendixes

### A.1 Table with variances

Table A.1: This is a Table with Data

Nr	$h[m]$	$\bar{U}[ms^{-1}]$	$T_w[s]$	$H_w[cm]$	NP	$\sigma_X^2[m^2s^{-2}]$	$\sigma_{X,T}^2[m^2s^{-2}]$	$SNR$	$V_{W_S,y}[ms^{-1}]$
12	0.15	2.0	2.10	50.0	3	0.17	4.22	0.04	0.49
12	0.30	2.0	2.10	50.0	3	0.56	7.15	0.08	0.58
12	0.45	2.0	2.10	50.0	3	0.70	15.61	0.04	0.79
12	0.60	2.0	2.10	50.0	3	2.06	8.22	0.25	1.35
12	0.75	2.0	2.10	50.0	3	0.95	5.26	0.18	1.54
12	0.90	2.0	2.10	50.0	3	0.34	3.98	0.09	1.78
12	1.41	2.0	2.10	50.0	3	0.03	0.46	0.06	1.98
12	2.22	2.0	2.10	50.0	3	0.09	1.10	0.08	2.15
12	3.03	2.0	2.10	50.0	3	0.01	1.78	0.01	2.14
13	0.15	3.0	2.10	50.0	3	0.30	20.39	0.01	0.68
13	0.30	3.0	2.10	50.0	3	0.48	19.83	0.02	0.74
13	0.45	3.0	2.10	50.0	3	1.51	31.72	0.05	1.18
13	0.60	3.0	2.10	50.0	3	0.39	12.92	0.03	2.13
13	0.75	3.0	2.10	50.0	3	0.96	11.95	0.08	2.42
13	0.90	3.0	2.10	50.0	3	1.40	6.21	0.23	2.70
13	1.41	3.0	2.10	50.0	3	0.76	1.61	0.47	2.94
13	2.22	3.0	2.10	50.0	3	0.17	2.12	0.08	3.23
13	3.03	3.0	2.10	50.0	3	0.02	3.37	0.01	3.18
14	0.15	4.0	2.10	50.0	3	0.19	43.19	0.00	0.86
14	0.30	4.0	2.10	50.0	3	0.32	37.59	0.01	0.82
14	0.45	4.0	2.10	50.0	3	4.89	45.54	0.11	1.58
14	0.60	4.0	2.10	50.0	3	1.77	36.75	0.05	2.69
14	0.75	4.0	2.10	50.0	3	0.63	42.04	0.02	3.18
14	0.90	4.0	2.10	50.0	3	3.03	26.72	0.11	3.63
14	1.40	4.0	2.10	50.0	3	1.20	4.52	0.27	4.02
14	2.22	4.0	2.10	50.0	3	0.19	6.92	0.03	4.43
14	3.03	4.0	2.10	50.0	3	0.01	6.64	0.00	4.26
17	0.75	2.0	1.15	8.0	7	0.03	2.67	0.01	1.90
17	0.15	2.0	1.15	8.0	7	0.07	19.72	0.00	0.42
17	0.30	2.0	1.15	8.0	7	0.07	40.90	0.00	0.52
17	0.45	2.0	1.15	8.0	7	0.21	38.05	0.01	1.07
17	0.60	2.0	1.15	8.0	7	0.27	7.08	0.04	1.62
17	0.75	2.0	1.15	8.0	7	0.06	4.12	0.01	1.77
17	0.90	2.0	1.15	8.0	7	0.04	0.77	0.05	1.99
17	1.41	2.0	1.15	8.0	7	0.01	0.24	0.06	1.97

17	2.22	2.0	1.15	8.0	7	0.00	0.49	0.00	2.16
17	3.03	2.0	1.15	8.0	7	0.01	0.80	0.01	2.09
18	0.15	2.0	1.60	8.0	4	0.07	2.88	0.02	0.61
18	0.30	2.0	1.60	8.0	4	0.24	2.84	0.09	0.74
18	0.45	2.0	1.60	8.0	4	0.31	2.45	0.12	1.13
18	0.60	2.0	1.60	8.0	4	0.09	1.91	0.05	1.52
18	0.75	2.0	1.60	8.0	4	0.02	1.77	0.01	1.81
18	0.90	2.0	1.60	8.0	4	0.05	0.55	0.08	1.98
18	1.41	2.0	1.60	8.0	4	0.01	0.20	0.05	1.98
18	2.22	2.0	1.60	8.0	4	0.00	0.26	0.00	2.15
18	3.03	2.0	1.60	8.0	4	0.00	0.64	0.00	2.11
19	0.15	2.0	1.96	8.0	3	0.11	1.91	0.06	0.56
19	0.30	2.0	1.96	8.0	3	0.31	2.48	0.12	0.82
19	0.45	2.0	1.96	8.0	3	0.46	2.14	0.21	1.07
19	0.60	2.0	1.96	8.0	3	0.58	2.29	0.25	1.44
19	0.75	2.0	1.96	8.0	3	0.01	1.14	0.01	1.73
19	0.90	2.0	1.96	8.0	3	0.03	0.68	0.04	1.94
19	1.40	2.0	1.96	8.0	3	0.01	0.50	0.01	1.98
19	2.22	2.0	1.96	8.0	3	0.00	6.29	0.00	2.22
19	3.03	2.0	1.96	8.0	3	0.01	175.47	0.00	2.36
20	0.15	2.0	2.26	8.0	3	0.13	2.86	0.05	0.67
20	0.30	2.0	2.26	8.0	3	0.11	3.49	0.03	0.94
20	0.45	2.0	2.26	8.0	3	0.41	2.29	0.18	1.14
20	0.60	2.0	2.26	8.0	3	0.27	1.74	0.15	1.48
20	0.75	2.0	2.26	8.0	3	0.39	3.28	0.12	1.71
20	0.90	2.0	2.26	8.0	3	0.12	2.27	0.05	1.88
20	1.40	2.0	2.26	8.0	3	0.05	0.35	0.16	1.98
20	2.22	2.0	2.26	8.0	3	0.00	0.31	0.00	2.13
20	3.03	2.0	2.26	8.0	3	0.01	0.85	0.01	2.10
21	0.32	2.0	1.60	8.0	4	0.02	1.01	0.02	0.32
21	0.34	2.0	1.60	8.0	4	0.10	2.29	0.04	0.74
21	0.46	2.0	1.60	8.0	4	0.25	2.38	0.11	1.18
21	0.75	2.0	1.60	8.0	4	0.09	1.61	0.05	1.76
21	0.85	2.0	1.60	8.0	4	0.01	1.80	0.01	1.89
21	1.05	2.0	1.60	8.0	4	0.05	0.55	0.08	2.06
21	1.35	2.0	1.60	8.0	4	0.02	0.28	0.07	2.00
21	1.65	2.0	1.60	8.0	4	0.00	0.31	0.01	2.03
21	1.95	2.0	1.60	8.0	4	0.01	0.34	0.03	2.18
21	2.25	2.0	1.60	8.0	4	0.00	0.42	0.00	2.13
21	2.55	2.0	1.60	8.0	4	0.00	1.01	0.00	2.07
21	2.85	2.0	1.60	8.0	4	0.00	0.84	0.00	2.15
21	3.15	2.0	1.60	8.0	4	0.03	1.67	0.02	2.12
21	3.45	2.0	1.60	8.0	4	0.13	5.80	0.02	2.12
22	0.15	2.0	2.26	8.0	3	0.24	3.53	0.07	0.58
22	0.45	2.0	2.26	8.0	3	0.77	2.63	0.29	1.18
22	0.75	2.0	2.26	8.0	3	0.18	1.97	0.09	1.71
22	0.85	2.0	2.26	8.0	3	0.04	2.75	0.01	1.87
22	1.05	2.0	2.26	8.0	3	0.11	0.66	0.16	2.03
22	1.35	2.0	2.26	8.0	3	0.05	0.58	0.08	1.99
22	1.65	2.0	2.26	8.0	3	0.00	2.87	0.00	2.07
22	1.95	2.0	2.26	8.0	3	0.00	1.74	0.00	2.13
22	2.25	2.0	2.26	8.0	3	0.00	0.45	0.01	2.13

22	2.55	2.0	2.26	8.0	3	0.00	0.67	0.00	2.05
22	2.85	2.0	2.26	8.0	3	0.00	0.75	0.00	2.16
22	3.15	2.0	2.26	8.0	3	0.00	1.69	0.00	2.10
22	3.45	2.0	2.26	8.0	3	0.09	38.80	0.00	2.13
23	0.15	2.0	2.53	8.0	4	1.43	6.51	0.22	0.70
23	0.45	2.0	2.53	8.0	4	1.05	5.89	0.18	1.08
23	0.75	2.0	2.53	8.0	4	0.12	5.14	0.02	1.74
23	0.85	2.0	2.53	8.0	4	0.07	3.40	0.02	1.86
23	1.05	2.0	2.53	8.0	4	0.23	1.06	0.21	2.02
23	1.35	2.0	2.53	8.0	4	0.29	1.16	0.25	2.02
23	1.65	2.0	2.53	8.0	4	0.01	2.61	0.00	2.07
23	1.95	2.0	2.53	8.0	4	0.00	2.59	0.00	2.14
23	2.25	2.0	2.53	8.0	4	0.00	0.90	0.00	2.13
23	2.55	2.0	2.53	8.0	4	0.00	1.30	0.00	2.07
23	2.85	2.0	2.53	8.0	4	0.00	1.52	0.00	2.16
23	3.15	2.0	2.53	8.0	4	0.02	2.56	0.01	2.15
23	3.45	2.0	2.53	8.0	4	0.25	17.06	0.01	2.08
24	0.15	2.0	2.77	8.0	4	0.96	5.77	0.17	0.64
24	0.45	2.0	2.77	8.0	4	1.57	4.76	0.33	1.13
24	0.75	2.0	2.77	8.0	4	0.50	5.01	0.10	1.70
24	0.85	2.0	2.77	8.0	4	0.30	3.77	0.08	1.80
24	1.05	2.0	2.77	8.0	4	0.35	2.28	0.15	2.00
24	1.35	2.0	2.77	8.0	4	0.29	1.99	0.14	2.00
24	1.65	2.0	2.77	8.0	4	0.03	3.19	0.01	2.04
24	1.95	2.0	2.77	8.0	4	0.01	0.56	0.02	2.14
24	2.25	2.0	2.77	8.0	4	0.01	1.00	0.01	2.11
24	2.55	2.0	2.77	8.0	4	0.01	1.73	0.00	2.07
24	2.85	2.0	2.77	8.0	4	0.01	1.72	0.01	2.17
24	3.15	2.0	2.77	8.0	4	0.02	2.99	0.01	2.10
24	3.45	2.0	2.77	8.0	4	0.10	23.46	0.00	2.11
25	0.15	2.0	3.00	8.0	3	1.98	4.22	0.47	0.74
25	0.45	2.0	3.00	8.0	3	1.55	4.03	0.38	1.08
25	0.75	2.0	3.00	8.0	3	0.59	5.39	0.11	1.62
25	0.85	2.0	3.00	8.0	3	1.13	6.43	0.18	1.71
25	1.05	2.0	3.00	8.0	3	0.25	1.76	0.14	2.01
25	1.35	2.0	3.00	8.0	3	0.30	0.46	0.66	1.99
25	1.65	2.0	3.00	8.0	3	0.03	0.48	0.06	2.03
25	1.95	2.0	3.00	8.0	3	0.03	0.34	0.08	2.13
25	2.25	2.0	3.00	8.0	3	0.02	0.66	0.03	2.15
25	2.55	2.0	3.00	8.0	3	0.01	1.05	0.01	2.07
25	2.85	2.0	3.00	8.0	3	0.03	1.05	0.03	2.13
25	3.15	2.0	3.00	8.0	3	0.06	4.34	0.01	2.15
25	3.45	2.0	3.00	8.0	3	0.00	23.13	0.00	2.04
26	0.15	2.0	3.20	8.0	3	1.19	6.56	0.18	0.82
26	0.45	2.0	3.20	8.0	3	1.77	4.06	0.44	1.16
26	0.75	2.0	3.20	8.0	3	1.25	5.65	0.22	1.60
26	0.85	2.0	3.20	8.0	3	0.47	7.15	0.07	1.80
26	1.05	2.0	3.20	8.0	3	0.39	1.76	0.22	2.01
26	1.35	2.0	3.20	8.0	3	0.33	1.08	0.31	2.02
26	1.65	2.0	3.20	8.0	3	0.09	8.05	0.01	2.06
26	1.95	2.0	3.20	8.0	3	0.01	4.97	0.00	2.16
26	2.25	2.0	3.20	8.0	3	0.07	0.90	0.07	2.13

26	2.55	2.0	3.20	8.0	3	0.06	1.27	0.05	2.08
26	2.85	2.0	3.20	8.0	3	0.09	1.18	0.07	2.14
26	3.15	2.0	3.20	8.0	3	0.05	3.25	0.01	2.12
26	3.45	2.0	3.20	8.0	3	0.13	27.23	0.00	2.02
27	0.15	2.0	3.50	8.0	3	1.50	10.07	0.15	0.83
27	0.45	2.0	3.50	8.0	3	2.52	7.57	0.33	1.10
27	0.75	2.0	3.50	8.0	3	1.44	6.52	0.22	1.65
27	0.85	2.0	3.50	8.0	3	0.27	6.53	0.04	1.86
27	1.05	2.0	3.50	8.0	3	0.43	1.87	0.23	2.01
27	1.35	2.0	3.50	8.0	3	0.39	0.60	0.64	1.98
27	1.65	2.0	3.50	8.0	3	0.14	0.63	0.22	2.03
27	1.95	2.0	3.50	8.0	3	0.07	0.48	0.15	2.13
27	2.25	2.0	3.50	8.0	3	0.07	0.86	0.08	2.11
27	2.55	2.0	3.50	8.0	3	0.06	1.34	0.05	2.06
27	2.85	2.0	3.50	8.0	3	0.08	1.24	0.07	2.14
27	3.15	2.0	3.50	8.0	3	0.06	3.79	0.02	2.12
27	3.45	2.0	3.50	8.0	3	0.23	49.29	0.00	2.00
28	0.15	2.0	2.26	16.0	5	1.97	7.27	0.27	0.64
28	0.45	2.0	2.26	16.0	5	2.02	6.16	0.33	1.09
28	0.75	2.0	2.26	16.0	5	0.55	4.56	0.12	1.64
28	0.85	2.0	2.26	16.0	5	0.12	2.69	0.05	1.83
28	1.05	2.0	2.26	16.0	5	0.06	1.75	0.03	1.98
28	1.35	2.0	2.26	16.0	5	0.16	0.79	0.21	2.01
28	1.65	2.0	2.26	16.0	5	0.01	0.65	0.02	2.04
28	1.95	2.0	2.26	16.0	5	0.04	1.97	0.02	2.19
28	2.25	2.0	2.26	16.0	5	0.01	1.08	0.01	2.15
28	2.55	2.0	2.26	16.0	5	0.01	1.84	0.00	2.07
28	2.85	2.0	2.26	16.0	5	0.00	1.62	0.00	2.16
28	3.15	2.0	2.26	16.0	5	0.02	3.85	0.01	2.12
28	3.45	2.0	2.26	16.0	5	0.17	30.71	0.01	2.12
29	0.15	2.0	2.77	16.0	4	1.68	5.03	0.33	0.79
29	0.45	2.0	2.77	16.0	4	1.95	4.37	0.45	1.10
29	0.75	2.0	2.77	16.0	4	0.81	3.75	0.22	1.64
29	0.85	2.0	2.77	16.0	4	0.62	3.00	0.21	1.75
29	1.05	2.0	2.77	16.0	4	0.56	3.00	0.19	1.94
29	1.35	2.0	2.77	16.0	4	0.37	1.35	0.27	2.04
29	1.65	2.0	2.77	16.0	4	0.04	3.08	0.01	2.10
29	1.95	2.0	2.77	16.0	4	0.03	4.61	0.01	2.16
29	2.25	2.0	2.77	16.0	4	0.06	0.76	0.07	2.10
29	2.55	2.0	2.77	16.0	4	0.04	1.38	0.03	2.06
29	2.85	2.0	2.77	16.0	4	0.07	1.58	0.05	2.18
29	3.15	2.0	2.77	16.0	4	0.10	3.46	0.03	2.12
29	3.45	2.0	2.77	16.0	4	0.09	54.53	0.00	1.99
30	0.15	2.0	2.26	50.0	5	0.00	5.08	0.00	0.31
30	0.45	2.0	2.26	50.0	5	0.10	13.61	0.01	0.71
30	0.75	2.0	2.26	50.0	5	1.48	7.16	0.21	1.56
30	0.85	2.0	2.26	50.0	5	1.58	7.73	0.20	1.70
30	1.05	2.0	2.26	50.0	5	0.43	2.67	0.16	1.88
30	1.35	2.0	2.26	50.0	5	0.24	0.86	0.28	1.97
30	1.65	2.0	2.26	50.0	5	0.24	0.80	0.30	2.01
30	1.95	2.0	2.26	50.0	5	0.34	0.95	0.36	2.09
30	2.25	2.0	2.26	50.0	5	0.13	1.10	0.12	2.10

30	2.55	2.0	2.26	50.0	5	0.09	1.96	0.05	2.05
30	2.85	2.0	2.26	50.0	5	0.13	1.68	0.08	2.11
30	3.15	2.0	2.26	50.0	5	0.05	4.35	0.01	2.13
30	3.45	2.0	2.26	50.0	5	0.09	57.89	0.00	2.04

## A.2 PSD plots

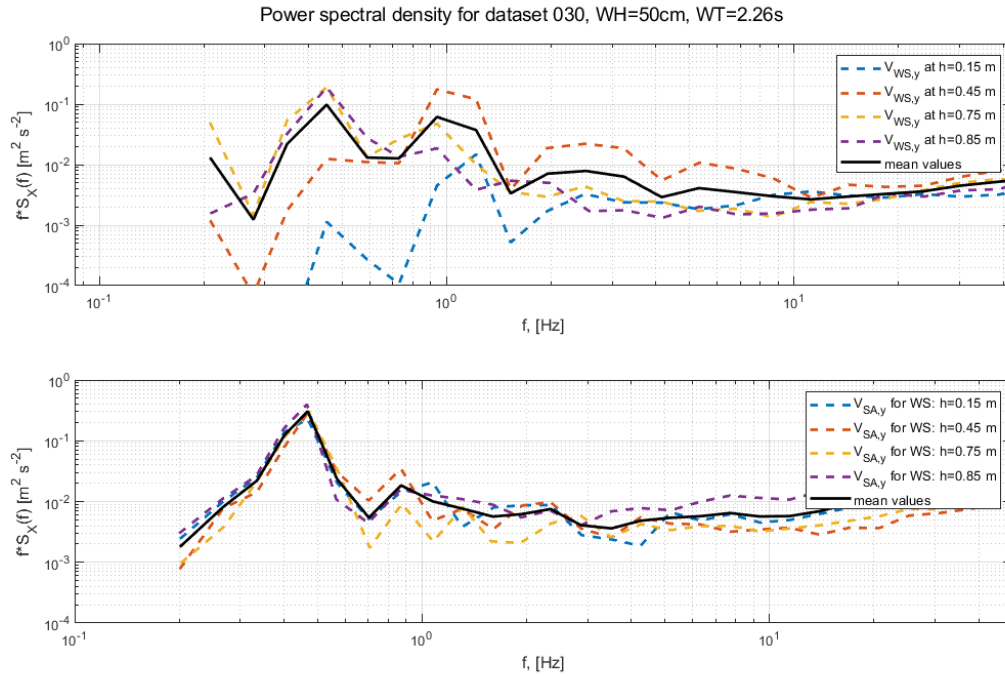


Figure A.1: Results from WindScanner and sonic anemometer for dataset nr. 30, heights 0.15-0.85m

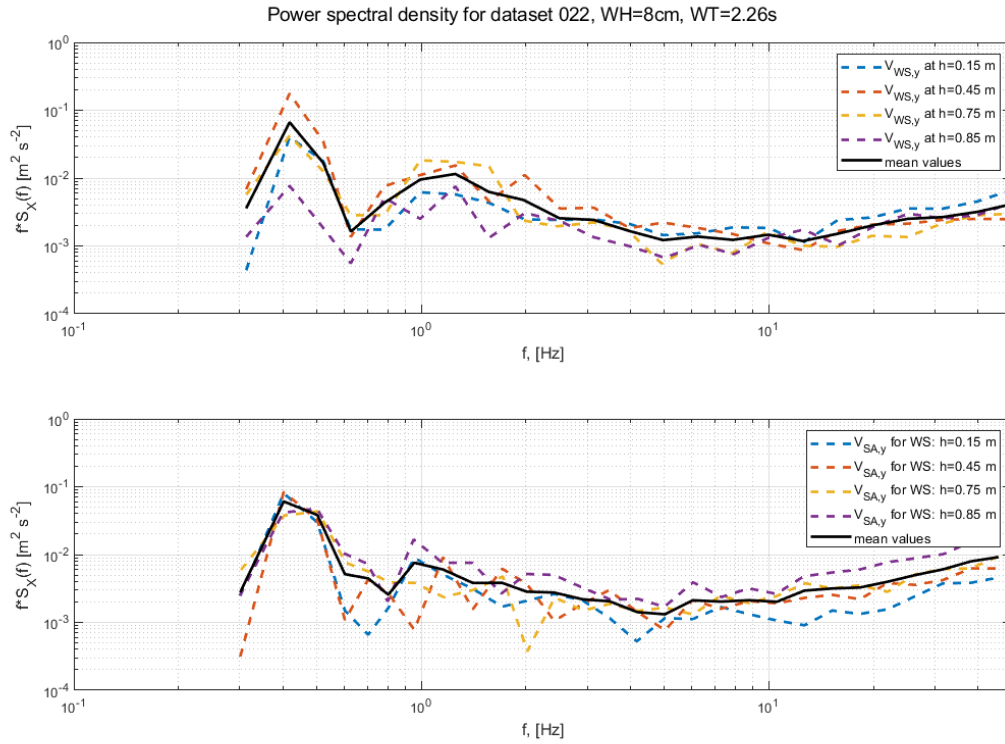


Figure A.2: Results from WindScanner and sonic anemometer for dataset nr. 22, heights 0.15-0.85m

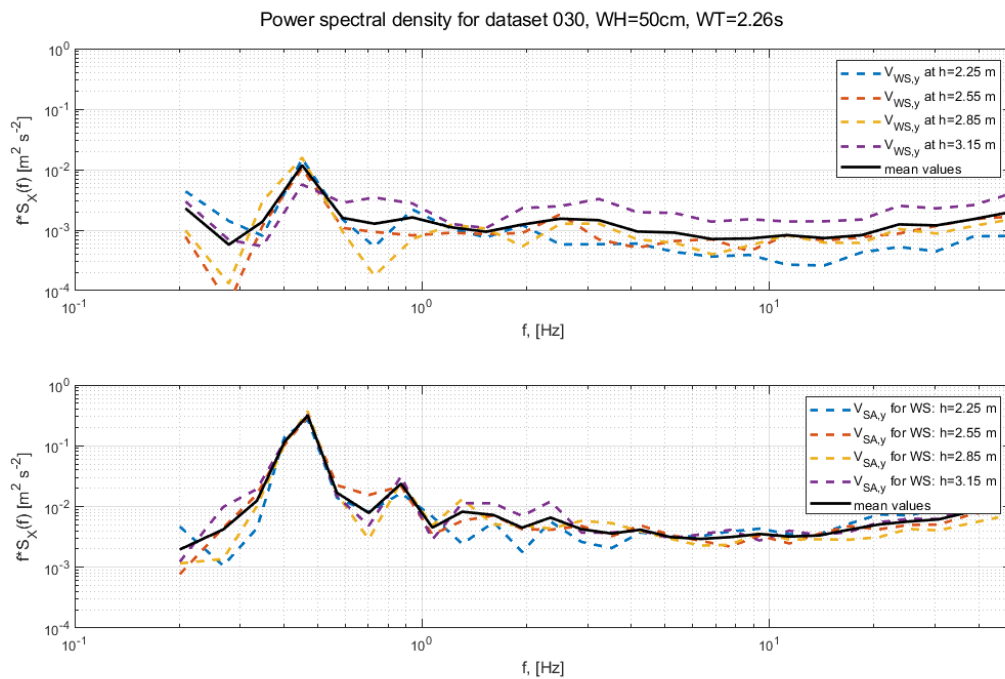


Figure A.3: Results from WindScanner and sonic anemometer for dataset nr. 30, heights 2.25-3.15m

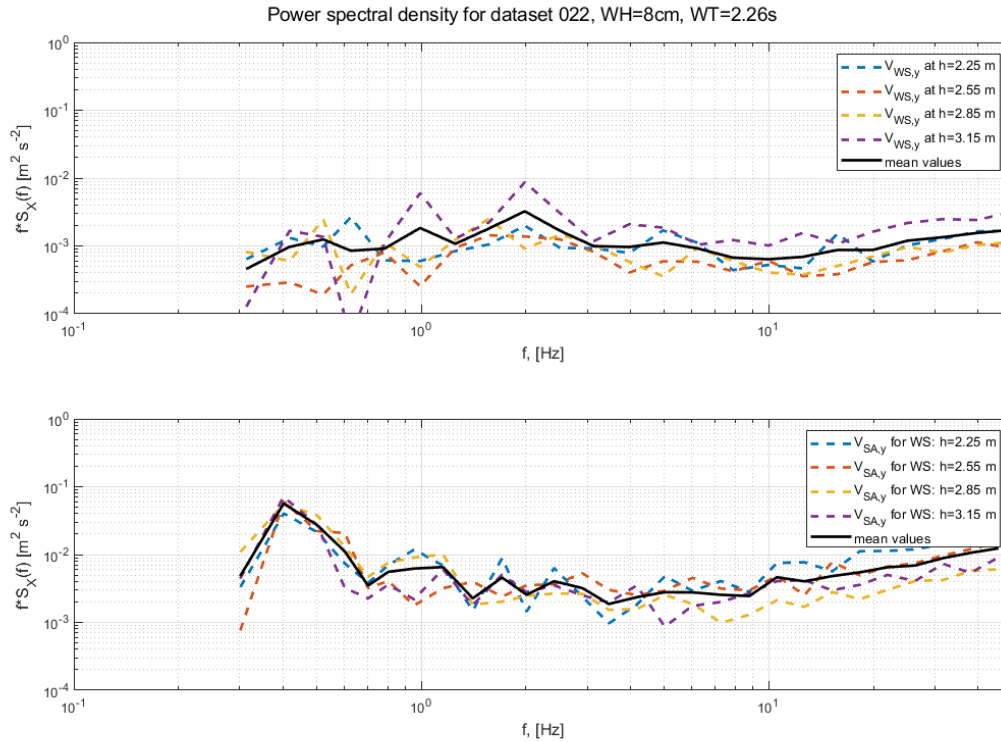


Figure A.4: Results from WindScanner and sonic anemometer for dataset nr. 22., heights 2.25-3.15m

### A.3 Matlab codes

Below the Matlab code to do a Fourier transform. The two input variables are the full wind data signal with a specific sampling frequency. The scaling is explained in Section 2.3.

```
function [f,S] = cospectra_onesided(signal,fs)
    % Function to evaluate the one-sided wind cospectra
    % signal is the wind measurement will be assessed
    % fs is the sampling rate
    N=length(signal);
    f=0:fs/N:fs/2; % frequency domain until the Nyquist frequency (fs/2)
    % Remember that the f=0 is the mean contribution, to be removed
    XX=fft(signal); % FFT over the time series
    I=floor(N/2)+1; %put it into closest integer
    X=XX(1:I); % pick only signal until the Nyquist frequency (fs/2)
    S= X.*conj(X); % Square of the transform
    S(1)=[]; f(1)=[]; % Remove the mean contribution where f=0
    % Scale according to 3.9.15 + account for the one-sided spectra (2x)
    S=(2*S)/(N*fs);
end
```

A.4 Pictures set-up



Figure A.5: This picture shows the tall standing propagating waves

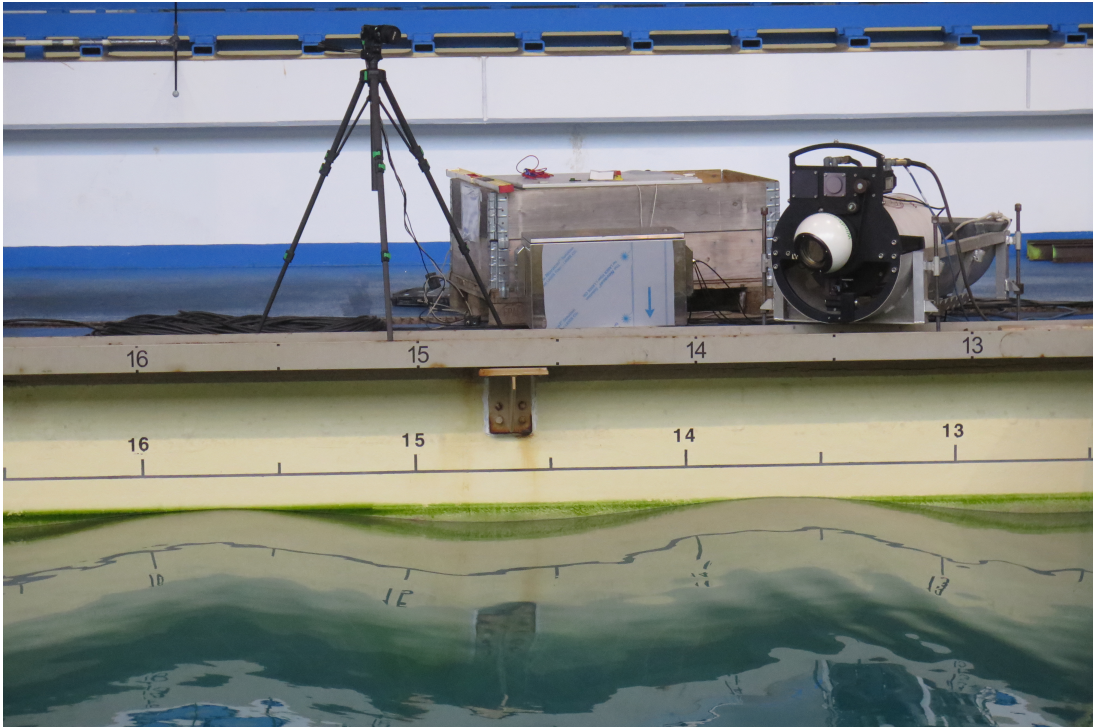


Figure A.6: Close picture of the R2D1 WindScanner

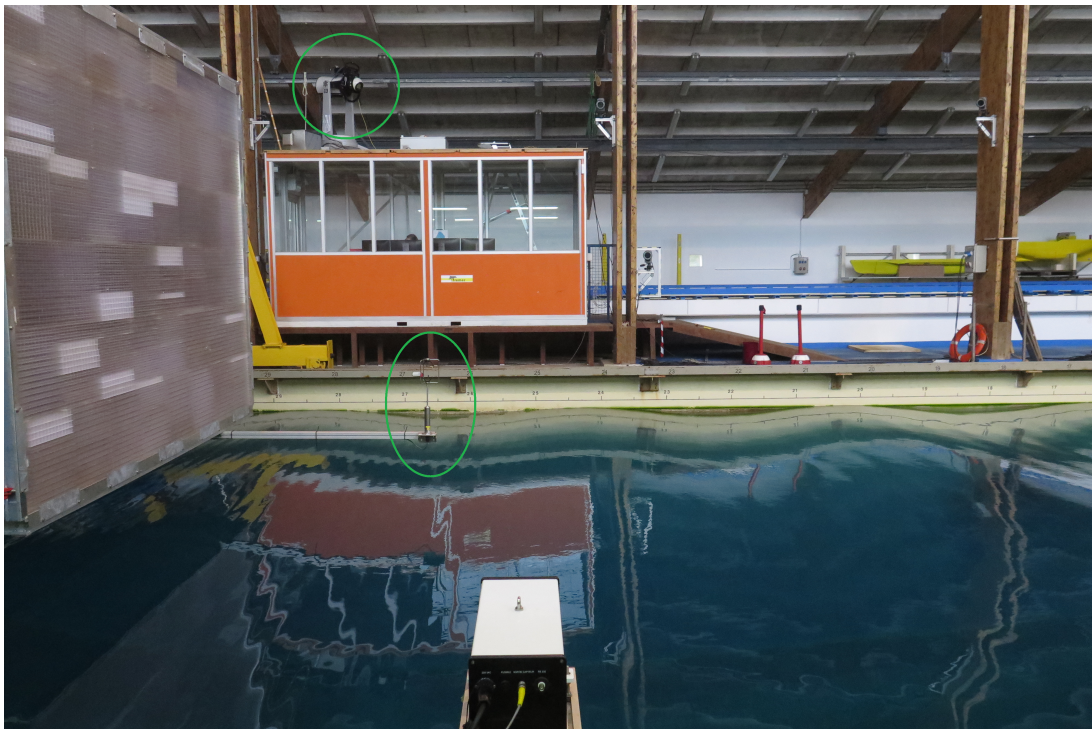


Figure A.7: Side view of the set up, in the front of the picture is the wave position measurement tool. On top of the orange-colored room, R2D3 is placed. The sonic anemometer is attached to the rectangular fan.